SCIENTIFIC REPORTS

OPEN

SUBJECT AREAS:
NANOPHOTONICS AND PLASMONICS
ATOMIC AND MOLECULAR INTERACTIONS WITH PHOTONS
CHEMICAL PHYSICS
SERS

Received
9 January 2014

Accepted
9 May 2014

Published
24 June 2014

Correspondence and requests for materials should be addressed to M.T.S. (mtsun@iphy.ac.cn) or P.J.W. (pjwang@cnu.edu.cn)

Plasmon-driven sequential chemical reactions in an aqueous environment

Xin Zhang[1,2], Peijie Wang[1], Zhenglong Zhang[3,4], Yurui Fang[5] & Mengtao Sun[1,2]

[1]The Beijing Key Laboratory for Nano-Photonics and Nano-Structure, Department of Physics, Capital Normal University, Beijing 100048, People's Republic of China, [2]Beijing National Laboratory for Condensed Matter Physics, Institute of Physics, Chinese Academy of Sciences, P. O. Box 603-146, Beijing, 100190, People's Republic of China, [3]Leibniz Institute of Photonic Technology, Albert-Einstein-Str. 9, 07745 Jena, Germany, [4]Physical Chemistry, Friedrich-Schiller University Jena, Helmholtzweg, 07743 Jena, Germany, [5]Division of Bionanophotonics, Department of Applied Physics, Chalmers University of Technology, Gothenburg SE-412 96, Sweden.

Plasmon-driven sequential chemical reactions were successfully realized in an aqueous environment. In an electrochemical environment, sequential chemical reactions were driven by an applied potential and laser irradiation. Furthermore, the rate of the chemical reaction was controlled via pH, which provides indirect evidence that the hot electrons generated from plasmon decay play an important role in plasmon-driven chemical reactions. In acidic conditions, the hot electrons were captured by the abundant H^+ in the aqueous environment, which prevented the chemical reaction. The developed plasmon-driven chemical reactions in an aqueous environment will significantly expand the applications of plasmon chemistry and may provide a promising avenue for green chemistry using plasmon catalysis in aqueous environments under irradiation by sunlight.

Surface plasmon chemistry is becoming a fast-growing branch of catalysis chemistry[1–21] because surface plasmons can strongly harvest electromagnetic energy via localized surface plasmon resonance (LSPR) when light irradiates the metal nanostructures. The absorbed electromagnetic energy can be transferred to molecules to overcome reaction barriers in plasmon-driven chemical reactions[3,4,12,14,16]. Hot electrons have been reported to be generated from plasmon decay[22], which provides the electrons as well as the kinetic energy required for some chemical reactions. Indirect experimental evidence that electron-driven catalytic reactions can be mediated by LSPR excitation arises from experimental reports of bond-selective dissociation induced by hot electrons, such as in plasmonic nanoscissors during tip-enhanced Raman spectroscopy (TERS)[10,19] and surface-enhanced Raman scattering (SERS)[20] experiments.

Further experimental evidence is necessary to investigate this phenomenon. For example, chemical reactions can be well controlled by manipulation of the hot electron concentration in the external environment. However, whether hot electrons are active in aqueous environments is unknown. Furthermore, whether the hot electron concentration can be manipulated in the external aqueous environment via manipulation of the acidic or alkaline conditions is unknown. If the hot electron concentration could be effectively manipulated through control of the aqueous environment, then plasmon-driven chemical reactions could be well controlled. Abundant H^+ in the aqueous environment could effectively capture hot electrons, reducing the hot electron concentration and hindering chemical reactions. In an environment with abundant negative ions, hot electrons could be effectively increased, promoting plasmon-driven chemical reactions. This type of experimental evidence could elucidate the contribution of hot electrons to chemical reactions. Furthermore, the goal of this study was to achieve facile, plasmon-driven chemical reactions at low cost and on a large scale. The aforementioned issues are important in the field of plasmon-driven chemistry, and understanding them is a considerable challenge.

In this paper, we report plasmon-driven sequential chemical reactions in which the target molecules are chemically adsorbed onto a roughened Ag substrate in an electrochemical aqueous environment. We demonstrate control over the chemical reaction using applied potentials and laser irradiation. We performed controlled, plasmon-driven sequential chemical reactions under different aqueous environments (different pH values), which revealed the fundamental contribution of hot electrons to the chemical reaction. Our findings may provide a promising avenue for green chemistry through sunlight-induced plasmon catalysis in aqueous environments.

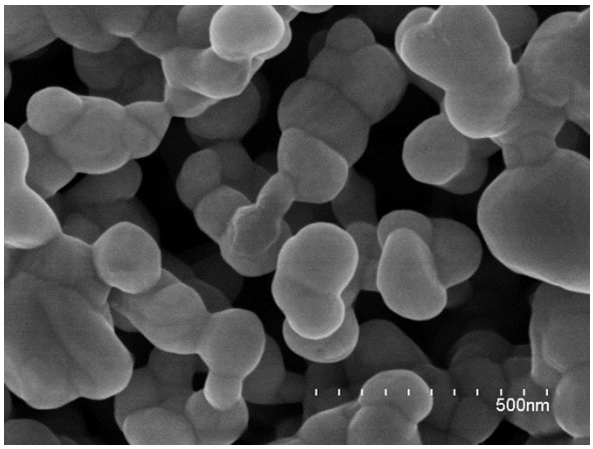

Figure 1 | An SEM image of the roughened Ag substrate.

Results

3D "hot spots" on the roughened substrate. The roughened Ag electrode can be observed on the nanoscale in the SEM image in Fig. 1, which shows three-dimensional (3D) "hot spots"[23] or 3D nanogaps. In the SEM image, the substrate is roughened not only along the surface but also perpendicular to the surface. 3D hot spots are known to produce stronger LSPR than ordinary 2D roughened substrates (i.e., substrates roughened only along the surface)[9,23]. This stronger LSPR is expected to enhance plasmon-driven chemical reactions in aqueous electrochemistry because 3D nanoparticles exhibit larger optical cross-sections and can selectively channel photon energies into small volumes known as hot spots, thereby enhancing local photocatalysis[24]. These 3D hot spots provide much higher rates of direct plasmonic photocatalysis compared to 2D hot spots.

Raman spectra of 4NTA. Figures 2(a) and 2(b) show the Raman spectra of 4-nitrothioanisole (4NTA) in water and 4NTA powder. Figure 2(c) is the calculated spectrum of 4NTA. Figures 2(d)–2(f) are the partial Raman spectra of Figs. 2(a)–2(c) in the range from 675 to 770 cm^{-1}. Theoretical calculations revealed three strong Raman peaks at 1091, 1338 and 1582 cm^{-1} as well as Raman peaks at 714 and 736 cm^{-1} in the low-frequency region (see Fig. 2(g)). The vibrational mode at 714 cm^{-1} was attributed to the S-CH_3 stretching mode. In the next section, we report that 4NTA can be converted into 4-nitrobenzenethiol (4NBT) by the dissociation of the CH_3 group of 4NTA on the SERS substrate.

SERS spectra of 4NTA at strong and weak laser powers. SERS spectra were measured on the electrode under high power (100%, 15 mW) laser irradiation in an aqueous environment (see Fig. 2(a)). We observed that the SERS spectra were significantly different from the Raman spectra in Fig. 2. However, when the laser power was weak (5%, 0.75 mW), the SERS spectra (see Figure 2(b)) were nearly identical to the Raman spectra in Fig. 2. Therefore, the SERS spectra of 4NTA were laser-power-dependent. The hot electron concentration is known to be strongly dependent on the laser power. By comparing Figs. 3(a) and 3(b), we can therefore conclude that the SERS spectra were dependent on the intensity of the LSPR[25] and that, with strong LSPR, the Raman spectra were produced from species catalyzed by LSPR. Theoretical calculations confirmed that 4NTA was catalytically reduced to DMAB (see Fig. 3(c)).

Potential-dependent plasmon-driven sequential chemical reactions. Figs. 3(a) and 3(b) reveal only one weak Raman peak at 724 cm^{-1}, whereas the spectra in Figs. 2(d)–(f) contain two weak Raman peaks. This difference occurred because of the dissociation of the S-CH_3 group of 4NTA, which adsorbed onto the substrate via a thiol bond, as observed by SERS. After the 4NTA adsorbed onto the Ag substrate, it was subsequently reduced to 4-nitrobenzenethiol (4NBT) via the dissociation of the CH_3 group from 4NTA, representing the first chemical reaction to occur; furthermore, this chemical reaction was irreversible. The oxidation-reduction potential provided further experimental evidence for this reaction.

To study the dynamics of plasmon-driven chemical reactions, we investigated the potential-dependent SERS spectra at weak (5%, 0.75 mV) laser power. Figure 4(a) reveals that when the potential was less than −0.4 V, no chemical reaction occurred for 4NBT; however, when the potential was greater than −0.9 V, a complete chemical reaction occurred. Between the potentials of −0.4 and −0.9 V, the chemical reaction was in progress and the SERS spectra included peaks from both 4NBT and DMAB. The scheme of the sequential, plasmon-driven chemical reaction is shown in Fig. 4(b).

To demonstrate that the plasmon-driven sequential chemical reactions were irreversible, we also decreased the potential gradually from −1.2 V to −0.1 V (see Fig. 4(c)). The chemical reaction was observed to be stable, as indicated by the presence of only DMAB peaks in the SERS spectra; this observation was confirmed by the simulated SERS spectrum of DMAB in Fig. 2(d). Therefore, the product catalyzed by the plasmon was stable and could not be reverted to 4NBT. Furthermore, only one Raman peak was observed, at 724 cm^{-1}, in Figs. 3(a) and 3(b), and no stretching mode from S-CH_3 was observed. Thus, the dissociation of S-CH_3 was also an irreversible chemical reaction.

Plasmon-driven chemical reactions revealed by oxidation-reduction potentials. To investigate the plasmon-driven chemical reactions, we also measured the oxidation-reduction potential. Notably, the redox properties of molecules are dependent on solvent effects[26].

Figure 5(a) shows the oxidation-reduction potential in the absence of 4NTA. Few peaks were present, indicating the absence of a reaction. After 4NTA was added to the aqueous phase (see Fig. 5(b)), we observed two oxidation-reduction (at 0.46 and 0.81 V). Therefore, two chemical reactions occurred, which we hypothesized to be the dissociation of S-CH_3 and the plasmon-driven conversion of 4NBT to DMAB. The peak at 0.46 V represents the dissociation of S-CH_3 because no DMAB was present in the samples shown in Fig. 3(c) and because only one Raman peak was observed (at 724 cm^{-1}). To demonstrate that the plasmon-driven chemical reactions were irreversible, we also further measured the oxidation-reduction potential after the processes represented in Figs. 5(a) and 5(b). No peaks were observed in Fig. 5(c), which confirms that the chemical reaction was complete in Fig. 4(a) and that the chemical reaction was stable and irreversible in Fig. 4(c). To provide further evidence that the peak at 0.46 V represents the dissociation of S-CH_3, we also measured the oxidation-reduction potential of thioanisole (see Fig. 5(d)). Only one peak was observed, at 0.46 V, which represented the dissociation of S-CH_3.

pH dependence of the plasmon-driven sequential chemical reactions. We also investigated the pH dependence of the plasmon-driven chemical reactions. Figure 6(a) shows the plasmon-driven irreversible chemical reactions at pH 3. Only the dissociation of the S-CH_3 group occurred, and the DMAB reaction was not catalyzed by LSPR. The plasmon-driven reaction was prevented by the abundant H^+ in the aqueous environment. The chemical reaction from 4NBT to DMAB requires four electrons per molecule. The hot electrons generated from the plasmon decay were captured by the abundant H^+. Fig. 6(b) shows the plasmon-driven chemical reactions at pH 10. The reaction proceeded more readily than in the neutral environment depicted in Fig. 4(a); the chemical reactions occurred at 0.3 V and were completed at 0.6 V. Thus, under alkaline conditions, the plasmon-driven chemical reaction requires

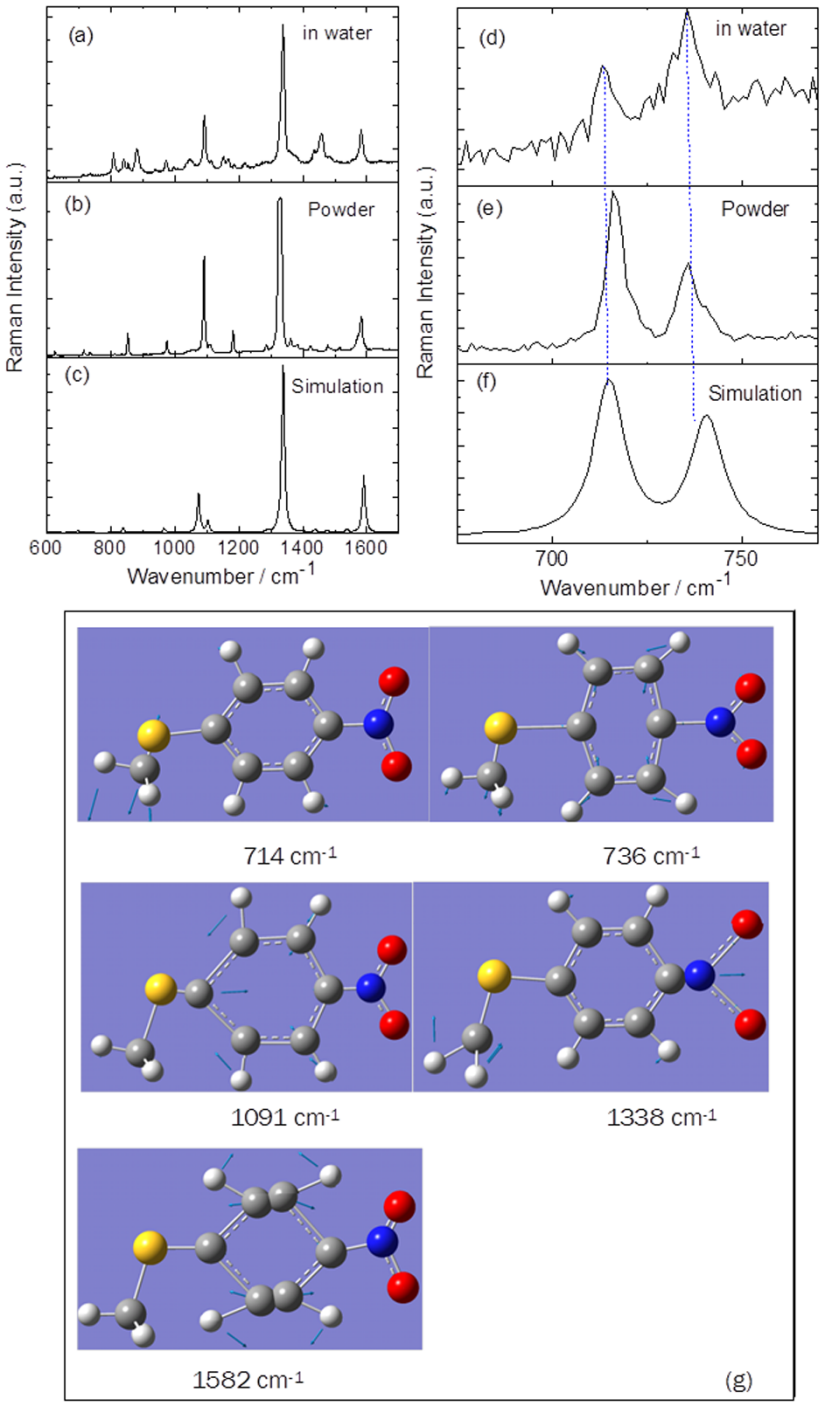

Figure 2 | Experimental and theoretical spectra of 4NTA. (a) The experimental Raman spectrum of 4NTA in water, (b) the experimental Raman spectrum of 4NTA powder, (c) the simulated Raman spectrum of 4NTA, (d)–(e) the Raman spectra from 675 to 770 cm^{-1} and (g) the vibrational modes in Figures 2(a)–2(f).

smaller voltage potentials because the OH^- groups favor the stability of the hot electrons generated from the plasmon decay, thereby facilitating the chemical reactions.

Discussion

We achieved plasmon-driven sequential chemical reactions, as confirmed by the dependence of electrochemical SERS measurements on laser intensity and by the oxidation-reduction potential measured by electrochemical SERS. The dissociation of the S-CH_3 group from 4NTA can be effectively catalyzed by LSPR. The laser-intensity dependence of the chemical reactions revealed that the chemical reactions required a large hot electron concentration. To produce a single DMAB, 4 hot electrons were needed. To force the chemical reactions to occur, a high hot electron concentration was necessary. Greater laser power resulted in the generation of more hot electrons from plasmon decay. These hot electrons surrounded the molecules and effectively promoted the chemical reactions.

The energy level of the hot electrons and the redox potential of the molecule were measured, along with the energy of the molecular reaction catalyzed by plasmon resonance (Fig. 7). Electron energy distributions are known to be time dependent and to follow the decay of a plasmon[27,28]. The depicted distributions in Fig. 7 are

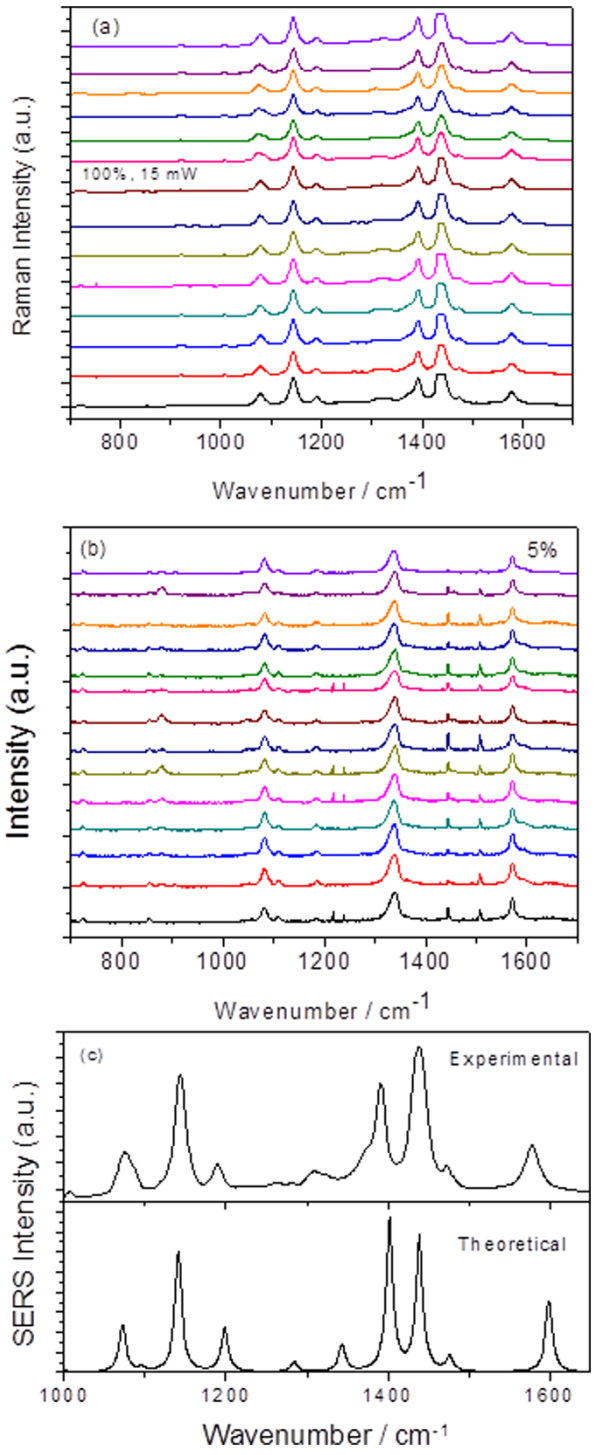

Figure 3 | Experimental and theoretical SERS spectra. (a) and (b) The SERS spectra of 4NTA under strong (100%, 15 mW) and weak (5%, 0.75 mW) laser power, respectively; (c) the experimental and theoretical spectra of DMAB, where the simulated SERS spectrum was taken from Ref. [1].

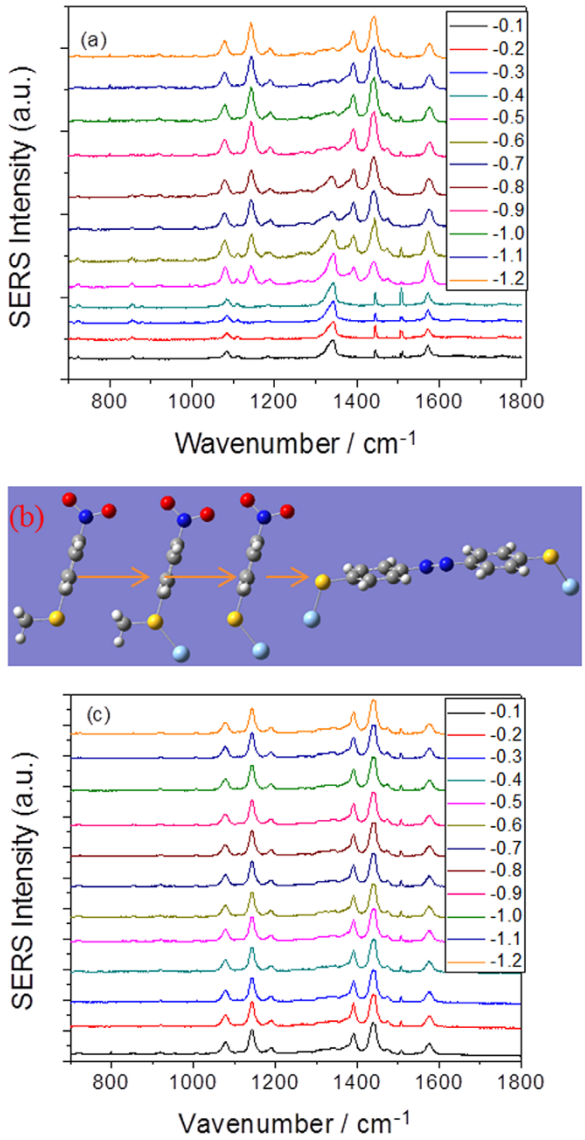

Figure 4 | Potential dependence of SERS. (a) Potential dependence of the SERS spectra with increasing potential from −0.1 to −1.2 V and (b) the potential dependence of the SERS spectra with decreasing potential from −1.2 to −0.1 V, excited with a 532 nm laser and weak laser power (5%, 0.75 mW).

time-averaged distributions[27,28]. Furthermore, the shapes of the distributions are very similar under weak and strong illumination and resembled a Fermi-Dirac distribution under these continuous wave CW illumination conditions[27,28]. The magnitude of the Fermi-Dirac distribution under these CW illumination conditions was strongly dependent on the laser intensity[28]. For a nanosystem, the carrier distribution has a large energy and occupies the entire region of $E_F < \varepsilon < E_F + \hbar\omega$, where E_F is the Fermi energy level. The physical reason for the aforementioned behavior is the non-conservation of momentum in a nanocrystal[28]. Thus, chemical reactions occur more readily under strong laser excitation than under weak laser excitation. Assisted by the electric potential, the total energy of the system was gradually increased, allowing chemical reactions to occur under weak laser excitation as well. Note that the relationship between the optical absorption energy and the shift of electrode potential can be estimated with[29]

$$E(\Delta V) = E_0(\Delta V = 0) - e\beta\Delta V \quad (1)$$

where $E(\Delta V)$ is the optical absorption energy with ΔV the change of the cathode potential V and $\beta \leq 1$. In the Helmholtz model, $\beta = 1$[30].

The chemical reactions were strongly dependent on the pH of the aqueous environment, which provided strong evidence for the role of the hot electrons generated from the plasmon decay in the chemical reaction. To produce a single DMAB molecule, four electrons are needed. In the acidic aqueous environment, the abundant H^+ captured most of the hot electrons generated by the plasmon decay,

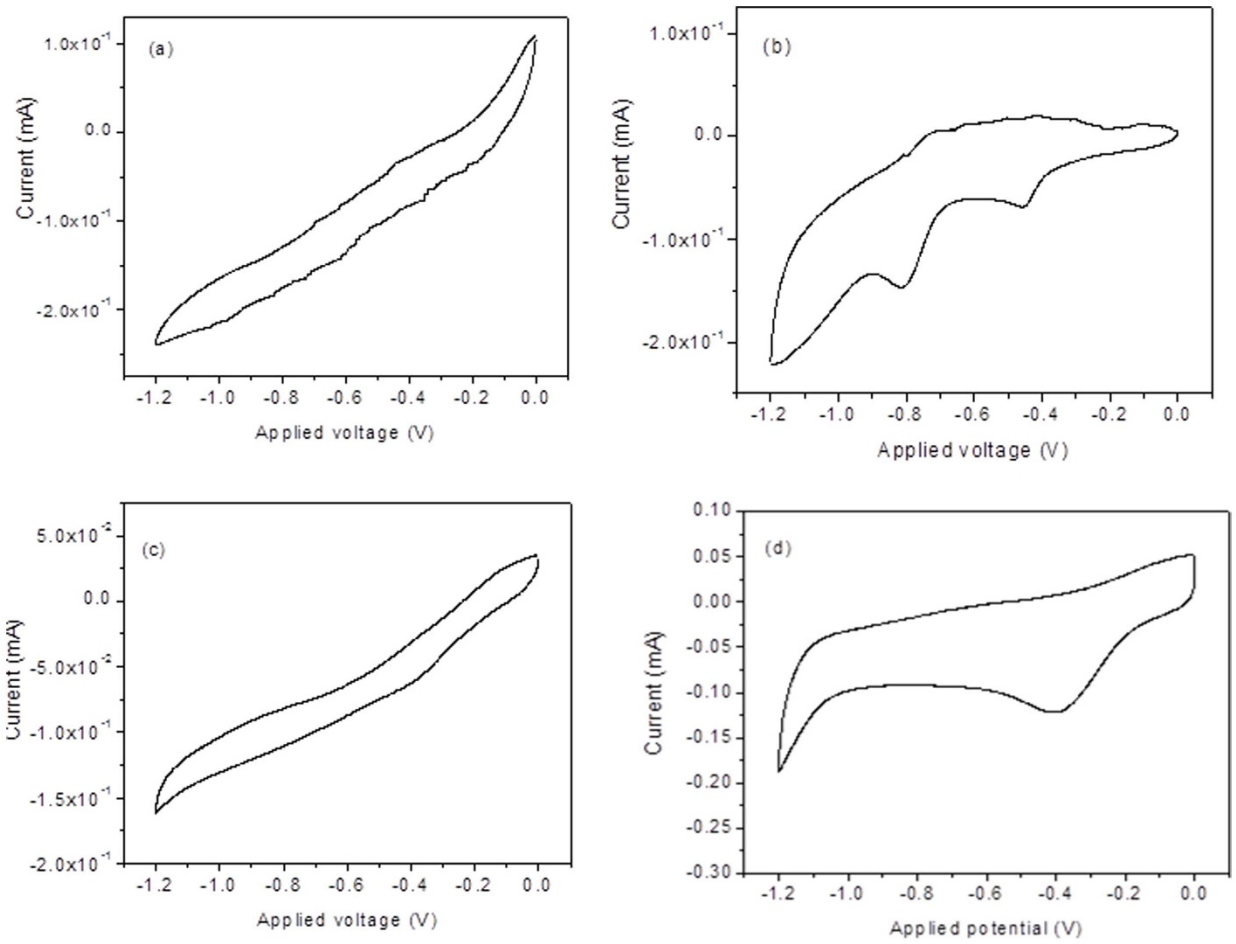

Figure 5 | **Cyclic voltammograms.** (a)–(c) Cyclic voltammograms without and with 4NTA and with 4NTA after the chemical reaction, respectively, and (d) the cyclic voltammograms of thioanisole.

thereby preventing chemical reactions from occurring. In the alkaline aqueous environment, the abundant OH^- effectively protected the hot electrons for the chemical reactions.

Heat generation by intense laser power tends to enhance chemical reactions; however, we avoided this phenomenon in the present work by reducing the laser intensity. The potential dependence of the chemical reactions in Fig. 4(a) were measured under weak (5%) laser power, where no chemical reactions could occur without the assistance of an applied electric potential (thereby demonstrating that the laser did not induce a heating effect); an increase in the electric potential from 0.46 to 0.81 V triggered the sequential chemical reactions under the same weak laser intensity. Thus, in the experiments represented in Fig. 4(a), the effects of heating by the intense laser could be excluded.

To accelerate the plasmon-driven reduction reactions, which required hot electrons, an alkaline aqueous environment was needed

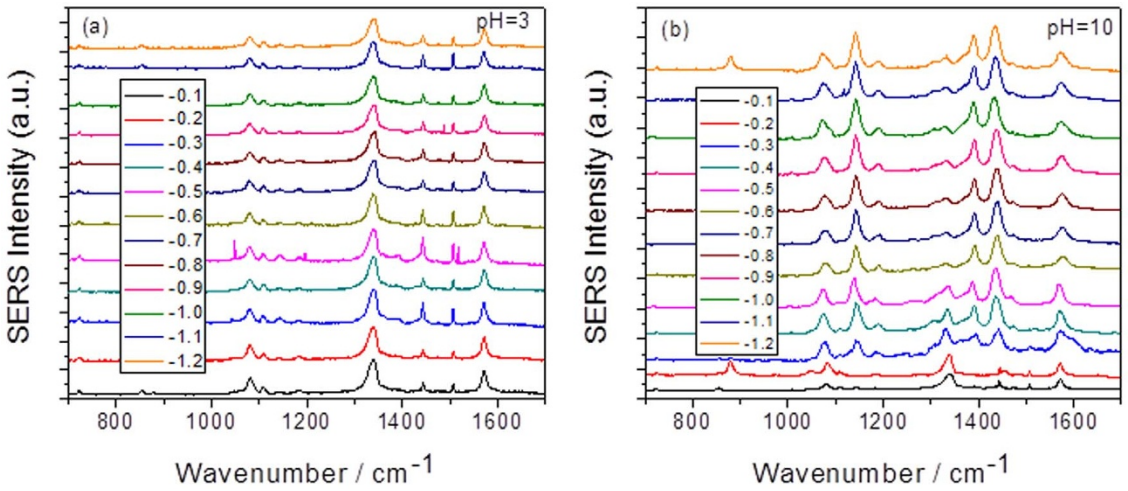

Figure 6 | **pH dependence of the plasmon-driven chemical reaction: (a) pH = 3 and (b) pH = 10.**

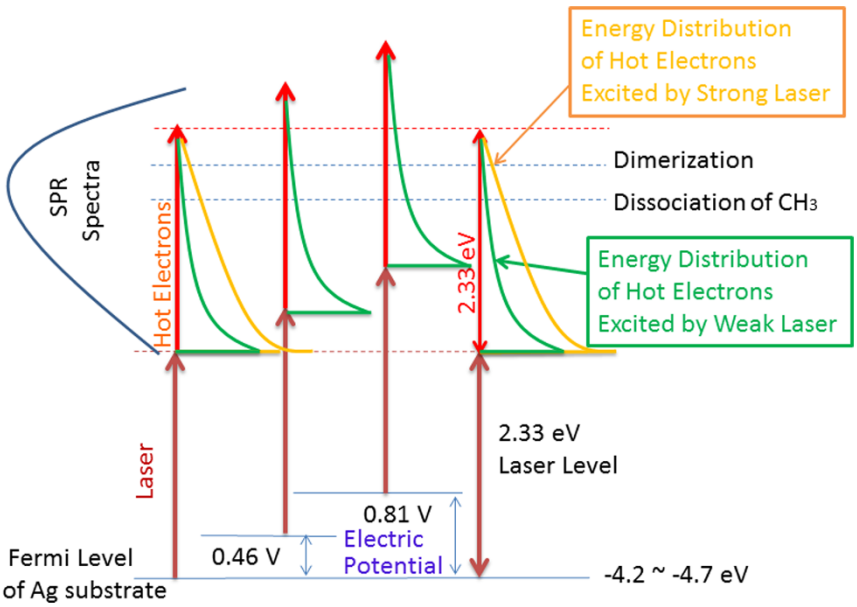

Figure 7 | The mechanism of the plasmon-driven sequential chemical reaction. The Fermi level of the Ag substrate was taken from the *CRC Handbook of Chemistry and Physics* (2008).

to protect the hot electrons. To prevent the plasmon-driven reduction reactions, acidic aqueous conditions were needed to capture the hot electrons generated by the plasmon decay using the abundant H^+ in the aqueous environment.

Methods

4NTA was purchased from Aldrich Chemical Co.. The Raman spectra of the 4NTA powder and of 4NTA in water (10^{-3} M) were measured with a Renishaw Invia spectrometer microprobe Raman system.

A three-electrode cell was used to perform the oxidation–reduction cycles (ORCs). The working electrode was a single-crystal silver rod of 99.9% purity, and a platinum wire was used as the counter electrode. An Ag/AgCl electrode was employed as the reference electrode.

The applied voltage of the working electrode was controlled by a CHI660A electrochemical instrument. The Raman spectra were recorded using a microprobe Raman system RH13325 (R-2000) spectrophotometer equipped with a high-sensitivity CCD detector. The samples were excited with a 532-nm laser with an effective power of 15 mW. A 50× objective was used to achieve a 180° backward scattering configuration.

Prior to the experiment, the Ag electrode was polished with emery paper and cleaned with Milli-Q water in an ultrasonic bath. It was placed in a typical electrochemical cell containing 0.1 M KCl solution for roughening. A double potential step was used to roughen the surface by applying a voltage of +0.25 V for 8 s and then applying a voltage of −0.35 V. This roughening treatment was applied to enhance the Raman intensity for the convenience of spectral recording.

After the roughening pretreatment, the electrode was placed in the electrochemical cell containing 0.1 M KCl and 0.1 M 4NTA solutions. The SEM imaging of the roughened Ag substrate was performed with a Hitachi S-4800. SERS spectra of 4NTA were collected on the electrode with a voltage ranging between 0 and −1.2 V.

The theoretical calculations of the molecular Raman spectra and their vibrational modes were performed with the Gaussian 09 software using density functional theory[31], the B3LYP functional[32] and 6-31G(d) basis set.

1. Fang, Y., Li, Y., Xu, H. & Sun, M. T. Ascertaining p,p′-Dimercaptoazobenzene Produced from p-Aminothiophenol by Selective Catalytic Coupling Reaction on Silver Nanoparticles. *Langmuir* **276**, 7737–7746 (2010).
2. Huang, Y. F. *et al.* When the signal is not from the original molecule to be detected: chemical transformation of para-aminothiophenol on Ag during the SERS measurement. *J. Am. Chem. Soc.* **132**, 9244–9246 (2010).
3. Christopher, P., Xin, H. & Linic, S. Visible-light-enhanced catalytic oxidation reactions on plasmonic silver nanostructures. *Nature. Chem.* **3**, 467–472 (2011).
4. Sun, M. T., Zhang, Z. L., Zheng, H. R. & Xu, H. X. In-situ plasmon-driven chemical reactions revealed by high vacuum tip-enhanced Raman spectroscopy. *Sci. Rep.* **2**, 647(2012).
5. Lantman, E. M. van S., Deckert-Gaudig, T., Mank, A. J. G., Deckert, V. & Weckhuysen, B. M. Catalytic processes monitored at the nanoscale with tip-enhanced Raman spectroscopy. *Nature Nanotech.* **7**, 583–586 (2012).
6. Sun, M. T. & Xu, H. X. A Novel Application of Plasmonics: Plasmon-Driven Surface-Catalyzed Reactions. *Small* **8**, 2777–2786 (2012).
7. Joseph, V. *et al.* Characterizing the Kinetics of Nanoparticle-Catalyzed Reactions by Surface-Enhanced Raman Scattering. *Angew. Chem. Int. Ed. Engl.* **51**, 7592–7596 (2012).
8. Ueno, K. & Misawa, H. Surface plasmon-enhanced photochemical reactions. *J. Photoch. Photobio.* **15**, 31–52 (2013).
9. Xie, W., Walkenfort, B. & Schlücker, S. Label-Free SERS Monitoring of Chemical Reactions Catalyzed by Small Gold Nanoparticles Using 3D Plasmonic Superstructures. *J. Am. Chem. Soc.* **135**, 1657–1660 (2013).
10. Sun, M. T., Zhang, Z. L., Kim, Z., Zheng, H. R. & Xu, H. X. Plasmonic Scissors for Molecular Design. *Chem. Eur. J.* **13**, 14958–14962 (2013).
11. Linic, S., Christopher, P., Xin, H. & Marimuthu, A. Catalytic and photocatalytic transformations on metal nanoparticles with targeted geometric and plasmonic properties. *Acc. Chem. Res.* **46**, 1890–1899 (2013).
12. Xiao, M. *et al.* Plasmon-enhanced chemical reactions. *J. Mater. Chem. A* **1**, 5790–5805 (2013).
13. Xu, P. *et al.* Mechanistic understanding of surface plasmon assisted catalysis on a single particle: cyclic redox of 4-aminothiophenol. *Sci. Rep.* **3**, 2997 (2013).
14. Mukherjee, S. *et al.* Hot Electrons Do the Impossible: Plasmon-Induced Dissociation of H_2 on Au. *Nano Lett.* **13**, 240–247 (2013).
15. Salmistraro, M. *et al.* Triggering and Monitoring Plasmon-Enhanced Reactions by Optical Nanoantennas Coupled to Photocatalytic Beads. *Small* **9**, 3301–3307 (2013).
16. Zhang, Z. *et al.* Insights into the nature of plasmon-driven catalytic reactions revealed by HV-TERS. *Nanoscale* **5**, 3249–3252 (2013).
17. Pincella, F., Isozaki, K. & Miki K. A visible light-driven plasmonic photocatalyst. *Light: Science & Application* **3**, e133 (2014).
18. Salmistraro, M. *et al.* Triggering and Monitoring Plasmon-Enhanced Reactions by Optical Nanoantennas Coupled to Photocatalytic Beads. *Small* **9**, 3301–3307 (2013).
19. Zhang, Z. L. *et al.* Molecular resonant dissociation of surface adsorbed molecules by plasmonic nanoscissors. *Nanoscale* **6**, 4903–4908 (2014).
20. Kim, K., Kim, K. L. & Shin, K. S. Photoreduction of 4,4′-Dimercaptoazobenzene on Ag Revealed by Raman Scattering Spectroscopy. *Langmuir* **29**, 183–190 (2013).
21. Sun, M. T. *et al.* Plasmon-driven selective reductions revealed by tip-enhanced Raman spectroscopy. *Adv. Mater. Int.* **1**, in press, (2014). DOI: 10.1002/admi: 201300125.
22. Knight, M. W., Sobhani, H., Nordlander, P. & Halas, N. J. Photodetection with active optical antennas. *Science* **332**, 702–704 (2011).
23. Urban, A. S. *et al.* Three-Dimensional Plasmonic Nanoclusters. *Nano Lett.* **13**, 4399–4403 (2013).
24. Michaels, A. M. & Brus, L. Ag Nanocrystal Junctions as the Site for Surface-Enhanced Raman Scattering of Single Rhodamine 6G Molecules. *J. Phys. Chem. B* **104**, 11965–11971 (2000).
25. Christopher, P., Xin, H., Marimuthu, A. & Linic, S. Singular characteristics and unique chemical bond activation mechanisms of photocatalytic reactions on plasmonic nanostructures. *Nature Materials* **11**, 1044–1050 (2012).

26. Taras-Goslinska, K. & Jonsson, M. Solvent Effects on the Redox Properties of Thioethers. *J. Phys. Chem. A* **110**, 9513–9517 (2006).
27. Kale, M. J., Avanesian, T. & Christopher, P. Direct Photocatalysis by Plasmonic Nanostructures. *ACS Catal.* **4**, 116–128 (2014).
28. Govorov, A. O., Zhang, H. & Gunko, Y. K. Theory of Photoinjection of Hot Plasmonic Carriers from Metal Nanostructures into Semiconductors and Surface Molecules. *J. Phys. Chem. C* **117**, 16616–16631 (2013).
29. Arenas, J. F., Fernandez, D. J., Soto, J., Lopez, I. L. & Otero, J. C. Role of the Electrode Potential in the Charge-Transfer Mechanism of Surface-Enhanced Raman Scattering. *J. Phys. Chem. B* **107**, 13143–13149 (2003).
30. Brett, C. M. A. & Brett, A. M. O. *Electrochemistry: Principles, Methods and Applications*, Oxford University Press, Oxford, England, 1993.
31. Parr, R. G. & Yang, W. *Density-functional theory of atoms and molecules* (Oxford Univ. Press, Oxford, 1989).
32. Lee, C., Yang, W. & Parr, R. G. Development of the Colle-Salvetti correlation-energy formula into a functional of the electron density. *Phys. Rev. B* **37**, 785–789 (1988).

Acknowledgments

This work was supported by the National Natural Science Foundation of China (Grant Nos. 11374353, 11274149 and 21073124) and the Program of Shenyang Key Laboratory of Optoelectronic Materials and Technology (F12-254-1-00).

Author contributions

M.S. and P.W. supervised the project, and M.S. designed the experiments. X.Z. measured the SERS spectra experimentally. M.S., X.Z. and P.W. analyzed the data. M.T.S. wrote the paper, and Z.Z. and Y.F. discussed and revised the manuscript.

Additional information

Competing financial interests: The authors declare no competing financial interests.

How to cite this article: Zhang, X., Wang, P., Zhang, Z., Fang, Y. & Sun, M. Plasmon-driven sequential chemical reactions in an aqueous environment. *Sci. Rep.* **4**, 5407; DOI:10.1038/srep05407 (2014).

This work is licensed under a Creative Commons Attribution-NonCommercial-ShareAlike 4.0 International License. The images or other third party material in this article are included in the article's Creative Commons license, unless indicated otherwise in the credit line; if the material is not included under the Creative Commons license, users will need to obtain permission from the license holder in order to reproduce the material. To view a copy of this license, visit http://creativecommons.org/licenses/by-nc-sa/4.0/